

## Joint propagation of short laser pulses in the $\Lambda$ -scheme of degenerated quantum transitions

© O.M. Parshkov, I.A. Plehanova

Yuri Gagarin State Technical University of Saratov,  
410054 Saratov, Russia

e-mail: oparshkov@mail.ru

Received May 19, 2023

Revised October 21, 2023

Accepted December 27, 2023

The conclusions of a theoretical study of the joint propagation in a resonant medium of two laser pulses with the same input intensity and envelope shape are reported. The resonant medium is modeled by the  $\Lambda$ -scheme of inhomogeneously broadened quantum transitions between degenerate levels  $^3P_0$ ,  $^3P_1^0$  and  $^3P_2$  of the  $^{208}\text{Pb}$  isotope. Cases of opposite and identical directions of circular polarizations of input fields are considered. It is shown that the process of pulse propagation is accompanied by a transfer of energy from the high-frequency component of the radiation, resonant with the transition between the lower and upper energy levels of the  $\Lambda$ -scheme, into the low-frequency component, resonant with the transition between excited levels and of the  $\Lambda$ -scheme. The high-frequency component in the case of different directions of circular polarizations of the input pulses propagates in the medium over a much greater distance than in the case of identical directions of circular polarizations of these pulses. During propagation, the pulse intensity envelopes are distorted, and in the case of opposite circular polarizations of the input pulses, the deformation of the envelopes is noticeably less than in the case of the same polarization directions of these pulses. In all cases, when pulses propagate, trains of short subpulses of significant intensity appear at their trailing edges. In the case of opposite directions of circular polarizations of the input fields, both radiations retain the original circular polarization in the medium and are devoid of phase modulation. However, in the case of identical directions of circular polarization of the input pulses, their radiation in the medium represents elliptically polarized waves with a variable eccentricity of the polarization ellipse and the presence of phase modulation.

**Keywords:** double resonance, electromagnetically induced transparency.

DOI: 10.61011/EOS.2023.12.58179.5228-23

### Introduction

Double resonance, i.e. resonant interaction of a two-frequency laser field with two quantum transitions having a common energy level, is the object of numerous studies due to the possibilities of its practical use and its importance for understanding the processes of interaction of radiation with matter. One of the first practical results of applying the findings of these studies was the double resonance method in spectroscopy [1]. The study of the phenomenon of coherent population trapping [2,3] and the resulting electromagnetically induced transparency (EIT) [4–6] effect (a special case of double resonance) has led to the development of optical memory [5], quantum communication [5,7,8], and quantum information systems [4–6], precision magnetic field measurement devices [9], and precision time measurement instruments [10]. The EIT phenomenon allows one to create large optical nonlinearities [6,11] and to implement radiation amplification without population inversion [12]. The features of this phenomenon have been studied in strongly correlated quantum gases [13], in the radio range [14], on impurities in photonic crystals [15], near nanofibers [16], and in a test field with orbital angular momentum [17].

In the theoretical study of double resonance, new pulse structures have been described, such as simultons [18], Raman solitons [19], adiabats [20], and matched pulses [21]. The theory of the last three pulse structures was based on the schemes of non-degenerate uniformly broadened quantum transitions, whereas the soliton theory included also the transitions between degenerate energy levels [22]; in [23], the inhomogeneous broadening of quantum transition lines was also taken into account. The experimental observation of these pulse structures required such conditions that are difficult to implement in practice. For example, simultons, adiabats, and Raman solitons may be produced only at equal strengths of oscillators of quantum transitions. Matched pulses were obtained under the assumption of zero inhomogeneous broadening of quantum transition lines. Therefore, the focus of attention in the study of double resonance has shifted to the region of the EIT phenomenon under the adiabatic approximation conditions [24].

In the case of degeneracy of quantum transition levels, the EIT effect demonstrates new features related to polarizations of interacting waves. In [25,26], the rotation of the plane of polarization of probe radiation with changing intensity of the control radiation field was studied theoretically and experimentally. Linear and circular birefringence

of a probe field under EIT was studied theoretically and experimentally in [27]. The possibility of propagation of a probe field in the form of two modes with different polarization states was predicted theoretically in [28].

The use of the adiabatic approximation implies rather slow changes in the parameters of interacting pulses and is unable to describe their fast oscillations, which, as numerical analysis [29] shows, can occur in this case. Notably, it was assumed in [29] that the levels of quantum transitions are not degenerate and there is no inhomogeneous broadening of quantum transition lines.

The present study reports the results of numerical analysis of the double resonance process in the  $\Lambda$  scheme formed by levels  $^3P_0$ ,  $^3P_2$ , and  $^3P_1^0$  of a  $^{208}\text{Pb}$  isotope. EIT of circularly polarized laser fields [30,31] was observed experimentally in this scheme. It is assumed that interacting pulses have the same peak intensities on entry to the medium and the duration of the input high-frequency (RF) pulse is equal to or twice the duration of the input low-frequency (LF) pulse. The degeneracy of energy levels and the presence of inhomogeneous broadening of spectral lines are taken into account. Note that the results of numerical analysis of the double resonance process in the considered  $\Lambda$  scheme in the case when the input RF pulse is significantly shorter than the input LF pulse were presented in [32].

## Basic concepts

The  $\Lambda$  scheme under study consists of a simple lower  $^3P_0$  level, a fivefold degenerate middle  $^3P_2$  level, and a threefold degenerate upper  $^3P_1^0$  level. We choose orthonormal basis  $\phi_k$  ( $k = 1, 2, \dots, 9$ ) of common eigenfunctions of the Hamiltonian, the square of the angular momentum, and its projection on axis  $z$ . Function  $\phi_1$  corresponds to level  $^3P_0$ ; functions  $\phi_k$  ( $k = 5, 6, \dots, 9$ ), to the states of level  $^3P_2$  ( $M = -2, -1, 0, 1, 2$ ); functions  $\phi_k$  ( $k = 2, 3, 4$ ), to the states of level  $^3P_1^0$ . Let  $D_1$  and  $D_2$  be the reduced dipole moments of RF transition  $^3P_0 \rightarrow ^3P_1^0$  and LF transition  $^3P_2 \rightarrow ^3P_1^0$  and  $\omega_1$  and  $\omega_2$  ( $\omega_1 > \omega_2$ ) be the frequencies of these transitions for an atom at rest. We take into account the heterogeneous broadening of spectral lines by introducing Gaussian density  $g(\omega'_1)$  of the distribution of frequencies  $\omega'_1$  of transitions  $^3P_0 \rightarrow ^3P_1^0$  of moving atoms:

$$g(\omega'_1) = (T_1/\sqrt{\pi}) \exp[-T_1^2(\omega'_1 - \omega_1)^2].$$

Let us write the electric field strength in the medium as  $\mathbf{E} = \mathbf{E}_1 + \mathbf{E}_2$ ,

$$\mathbf{E}_l = \mu_l [\mathbf{e}_x E_{xl} \cos(\omega_l t - k_l z + \delta_{xl}) + \mathbf{e}_y E_{yl} \cos(\omega_l t - k_l z + \delta_{yl})],$$

$$l = 1, 2. \quad (1)$$

Here,  $\mathbf{E}_l$  and  $\omega_l$  are the electric field strength and the carrier frequency of radiation;  $\mathbf{e}_x, \mathbf{e}_y$  are unit vectors of axes  $x, y, E_{xl}, E_{yl}$ ;  $\delta_{xl}, \delta_{yl}$  ( $-\pi \leq \delta_{xl}, \delta_{yl} \leq \pi$ ) are the amplitudes and are the phase additions of  $x$  and  $y$  components of fields describing their phase modulation

(PM);  $\mu_l = \hbar\sqrt{2l+1}/(|D_l|T_1)$ ; and  $k_l = \omega_l/c$ . At  $l = 1$ , formula (1) describes RF radiation resonant with transition  $^3P_0 \rightarrow ^3P_1^0$  between the ground and upper levels. At  $l = 2$ , formula (1) describes LF radiation resonant with transition  $^3P_2 \rightarrow ^3P_1^0$  between the middle and upper levels.

Let us introduce new independent variables  $s$  and  $w$ :

$$s = z/z_0, \quad w = (t - z/c)/T_1,$$

where  $z_0 = 3\hbar c/(2\pi N|D_1|^2 T_1 \omega_1)$  and  $N$  is the concentration of atoms. Let  $f_l$  and  $g_l$  be the complex amplitudes of circular components of fields. Using Maxwell and Schrödinger equations, we obtain the following system of equations in the first approximation of the slow envelope method:

$$\begin{aligned} \frac{\partial f_1}{\partial s} &= \frac{i}{\sqrt{\pi}} \int_{-\infty}^{+\infty} c_1 c_2^* \exp(-\varepsilon_1^2) d\varepsilon_1, \\ \frac{\partial f_2}{\partial s} &= -\frac{i}{\sqrt{\pi}} \xi \int_{-\infty}^{+\infty} (c_4^* c_9 + c_2^* c_7) \exp(-\varepsilon_1^2) d\varepsilon_1, \\ \frac{\partial g_1}{\partial s} &= -\frac{i}{\sqrt{\pi}} \int_{-\infty}^{+\infty} c_1 c_4^* \exp(-\varepsilon_1^2) d\varepsilon_1, \\ \frac{\partial g_2}{\partial s} &= \frac{i}{\sqrt{\pi}} \xi \int_{-\infty}^{+\infty} (c_2^* c_5 + c_4^* c_7) \exp(-\varepsilon_1^2) d\varepsilon_1, \\ \frac{\partial c_1}{\partial w} &= -i(f_1 c_2 - g_1 c_4), \\ \frac{\partial c_2}{\partial w} + i\varepsilon_1 c_2 &= -\frac{i}{4} (f_1^* c_1 + g_2^* c_5 - f_2^* c_7) - \gamma c_2, \\ \frac{\partial c_4}{\partial w} + i\varepsilon_1 c_4 &= \frac{i}{4} (g_1^* c_1 - g_2^* c_7 + f_2^* c_9) - \gamma c_4, \\ \frac{\partial c_5}{\partial w} + i(\varepsilon_1 - \varepsilon_2) c_5 &= -ig_2 c_2, \\ \frac{\partial c_7}{\partial w} + i(\varepsilon_1 - \varepsilon_2) c_7 &= \frac{i}{6} (f_2 c_2 - g_2 c_4), \\ \frac{\partial c_9}{\partial w} + i(\varepsilon_1 - \varepsilon_2) c_9 &= if_2 c_4. \end{aligned} \quad (2)$$

The following notation was used in Eqs. (2):

$$\varepsilon_1 = (\omega'_1 - \omega_1)T_1/2, \quad \varepsilon_2 = \beta\varepsilon_1,$$

$$\beta = \omega_2/\omega_1, \quad \xi = 0.6\beta|D_2/D_1|^2,$$

$$c_1 = \frac{|D_1|}{2D_1^*} \bar{c}_1, \quad c_2 = \bar{c}_2, \quad c_4 = \bar{c}_4,$$

$$c_{5,9} = \frac{|D_2|}{2D_2} \bar{c}_{5,9}, \quad c_7 = \frac{\sqrt{6}}{2} \frac{|D_2|}{D_2} \bar{c}_7,$$

$\bar{c}_k$ ,  $k = 1, 2, 4, 5, 7, 9$  — amplitude of the probability of populating state  $k$ . (Due to the  $\Delta M = \pm 1$  selection rules, amplitudes  $\bar{c}_k$ ,  $k = 3, 6, 8$  are not included into system (2).)

Terms  $-\gamma c_2$ ,  $-\gamma c_4$ , where  $\gamma = T_1/(2\tau)$  and  $\tau$  is the radiation lifetime of level  ${}^3P_1^0$ , are phenomenologically introduced into the equations to account for spontaneous decay of this level.

Usually, equations for the density operator are used to describe the response of the medium to resonant radiation. In the case of the  $\Lambda$  scheme under consideration, this means that there are 45 independent elements of the density matrix and the same number of differential equations for them. In connection with this, we use a less cumbersome system of equations derived from the Schrödinger equation. In this case, relaxation processes are accounted for phenomenologically by introducing terms describing the relaxation decay of the upper energy states of the  $\Lambda$  scheme. Note that such a consideration of relaxation processes leads to a decrease with time of the total number of atoms at levels of the  $\Lambda$  scheme. This is motivated physically. In the considered  $\Lambda$  scheme, the actual existing degenerate  ${}^3P_1$  energy level lying between the lower and middle levels of the  $\Lambda$  scheme is not taken into account. The transition between this level and the levels accounted for in our theory is not subject to the resonance influence of electromagnetic fields. However, it is coupled to the upper level of the  $\Lambda$  scheme by rather intense relaxation transitions. This leads to the fact that a certain number of atoms actually leave the levels of the  $\Lambda$  scheme, moving to level  ${}^3P_1$ . Note that relaxation processes at double resonance have been taken into account in a similar way in a considerable number of studies into double resonance (see, for example, [33,34]).

The following parameters of the polarization ellipse (PE) of RF ( $l = 1$ ) and LF ( $l = 2$ ) fields are used below:  $a_l$  is the semi-major axis of the PE in units of  $\mu_l$ ,  $\alpha_l$  ( $0 \leq \alpha_l \leq \pi$ ) is the angle between it and axis  $x$ , and  $\gamma_l$  is the compression parameter ( $-1 \leq \gamma_l \leq 1$ ). The modulus of  $\gamma_l$  is equal to the ratio of the minor PE axis to the major one;  $\gamma_l < 0$  ( $\gamma_l > 0$ ) if the polarization is right (left) elliptical. For circular polarization,  $\gamma_l = \pm 1$ , and  $\alpha_l$  is undefined and conventionally assumed to be equal to  $-0.1$ . Dimensionless intensities  $I_l$  of RF ( $l = 1$ ) and LF ( $l = 2$ ) fields measured in units of  $c\mu_l^2/(8\pi)$  will also be used.

When solving system (2), we assume that only the lower level  ${}^3P_0$  of  $\Lambda$ -scheme is populated at the initial moment of time ( $w = 0$ ). The boundary conditions are formulated by specifying quantities  $a_l$ ,  $\alpha_l$ ,  $\gamma_l$ ,  $\delta_{xl}$  as functions of variable  $w$  on the input surface of the medium ( $s = 0$ ):

$$\begin{aligned} a_1(0, w) &= a_{10} \operatorname{sech}[(w - 1000)/\tau_0], & \alpha_1(0, w) &= -0.1, \\ \gamma_1(0, w) &= \gamma_{10}, & \delta_{x1}(0, w) &= 0; \\ a_2(0, w) &= a_{20} \operatorname{sech}[(w - 1000)/100], & \alpha_2(0, w) &= -0.1, \\ \gamma_2(0, w) &= 1, & \delta_{x2}(0, w) &= 0. \end{aligned} \quad (4)$$

Here,  $a_{10} = 2.828$ ,  $a_{20} = 4.910$ , and  $\gamma_{10}$  will be assumed to be equal to  $\pm 1$ .

Formulae (3) describe an RF pulse with an intensity envelope in the form of an inverse hyperbolic cosine with parameter  $\tau_0$  determining the duration of this pulse. Below,

the value of  $\tau_0$  will be assumed to be 100 and 200. Formula (4) specifies an LF pulse with an intensity envelope of the same kind with a time parameter equal to 100. Pulses have the same peak intensity  $I_l = 16$ ,  $l = 1, 2$ . Both input pulses are devoid of PM.

According to [35],  $\omega_2/\omega_1 = 0.7$ ,  $\xi = 2.11$ ,  $\tau = 6$  ns, and (at  $T = 950\text{--}1050$  K)  $\gamma = 1.5 \cdot 10^{-2}$  in formulae (3), (4) for the chosen  ${}^{208}\text{Pb}$  transitions. At  $T = 1050$  K, we have  $T_1 = 1.6 \cdot 10^{-10}$  s. Choosing saturated  ${}^{208}\text{Pb}$  vapors for evaluation and using the data from [36], we find  $N = 2.8 \cdot 10^{14} \text{ cm}^{-3}$  and  $z_0 = 0.004$  cm at the same temperature. Note that  $z_0$  depends strongly on temperature, whereas the value of  $T_1$  is essentially unchanged within this temperature range. Below, all dimensional estimates are given for  $T = 1050$  K. Dimensionless intensity  $I_l$  is related to dimensional value  $\tilde{I}_l$  of this quantity as  $\tilde{I}_l = 1.3I_l \text{ kW/cm}^2$ , and its peak value at the entrance to the medium is close to  $20 \text{ kW/cm}^2$ . This was approximately the intensity of LF pulses in the experiments [30,31]. The duration of the input RF pulse is approximately 30 ns at  $\tau_0 = 100$  and 60 ns at  $\tau_0 = 200$ , while the input LF pulse has a duration of 30 ns. Here and below, pulse duration is measured at half peak intensity.

## Calculation results

### Input pulses of the same duration

(A) Input pulses with opposite polarization directions. Let us set  $\tau_0 = 100$  and  $\gamma_{10} = -1$  in (3). The input RF pulse has right circular polarization, the input LF pulse has left circular polarization, and the durations of these pulses are equal. Figure 1 shows plots of the values of  $I_l$  and  $\gamma_l$  ( $l = 1, 2$ ) at several distances  $s$ . For clarity, dashed lines represent the values of  $I_{l0}$  ( $l = 1, 2$ ), which is the intensity of a reference pulse (i.e., a pulse generated in empty space by the input radiation pulse). At all distances  $s$ , conditions  $\alpha_l = 0$  and  $\delta_{xl} = 0$  are fulfilled, so the plots of these quantities are not shown in Fig. 1. Note that  $s = 2000$  corresponds to a distance of 8 cm.

According to Fig. 1, the RF pulse gradually decays while propagating in the medium, while the LF radiation pulse intensifies, gaining energy from the RF pulse. At  $1500 < s < 2000$ , the propagation velocity of the peak of the RF pulse envelope is about 30 times lower than  $c$ . At the same distance, the maximum of the LF pulse envelope propagates with a velocity approximately equal to  $c$ . During propagation, the envelopes of both pulses deform significantly. At distance  $s = 2000$ , the RF pulse duration is about 16 ns, and the LF pulse duration is about 23 ns. According to Fig. 1, quantities  $\gamma_l$  ( $l = 1, 2$ ) remain constant at all distances and equal to their values at the input surface. Since quantities  $\alpha_l$ ,  $\delta_{xl}$  ( $l = 1, 2$ ) have the same property, we can conclude that both pulses have circular polarization and no PM.

As the pulses propagate in the medium, trains of short subpulses (Fig. 1,  $c, f$ ) with a sufficiently large peak

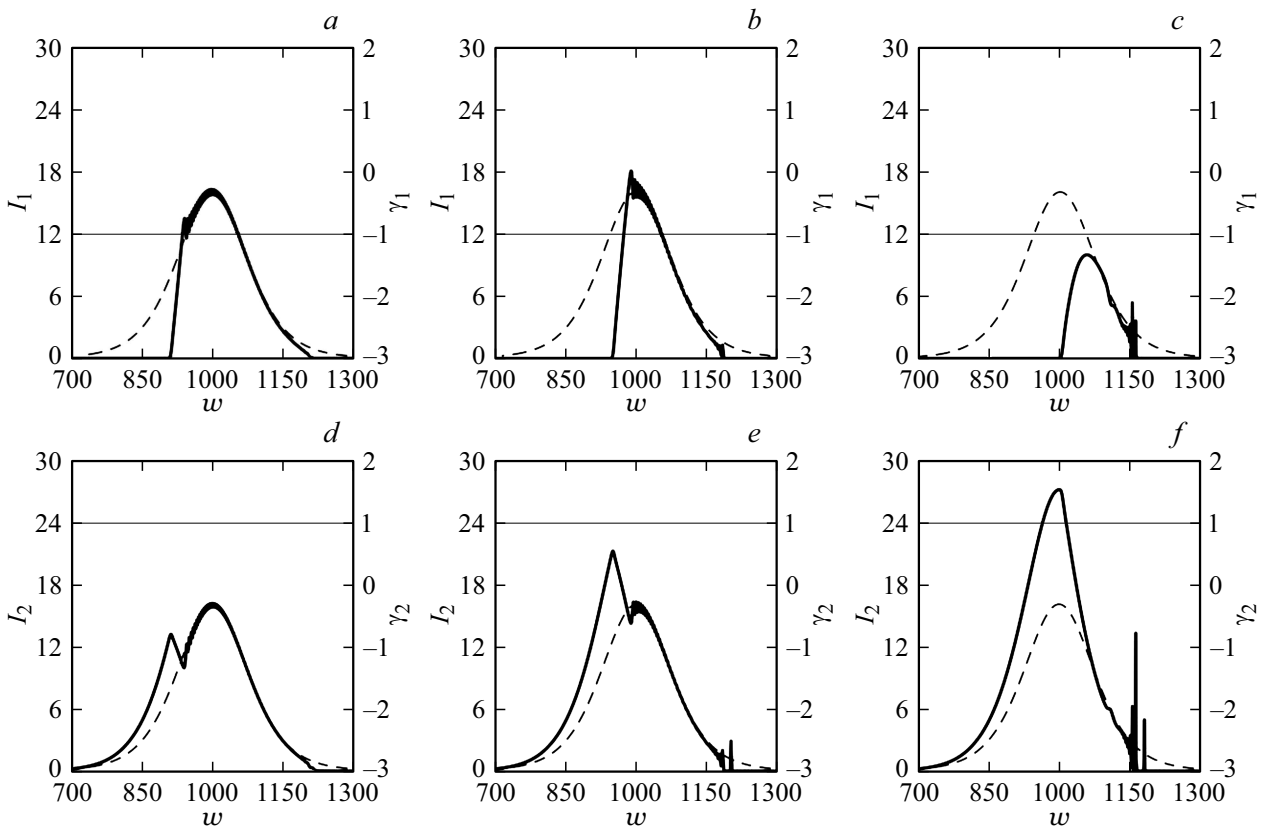


**Figure 1.** Evolution of the values of  $I_1$  (thick lines),  $\gamma_1$  (thin lines), and  $I_{10}$  (dashed lines) at  $s = 800$  (a),  $1000$  (b), and  $2000$  (c); evolution of the values of  $I_2$  (thick lines),  $\gamma_2$  (thin lines), and  $I_{20}$  (dashed lines) at  $s = 800$  (d),  $1000$  (e), and  $2000$  (f).

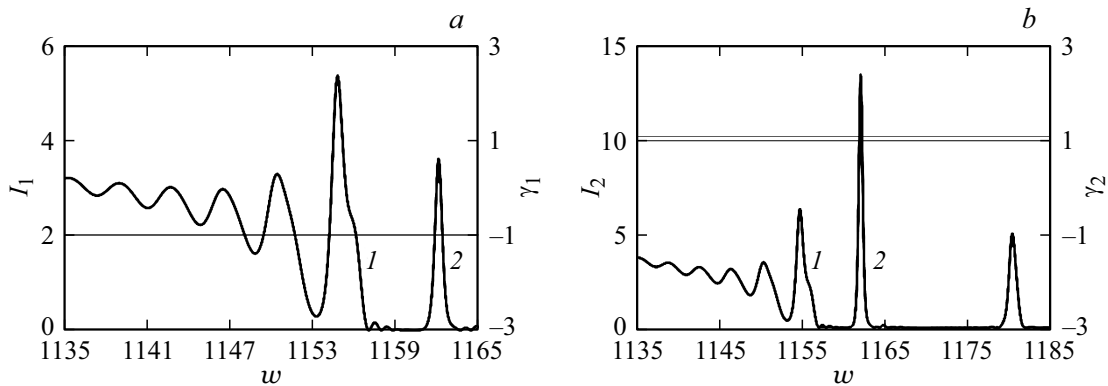


**Figure 2.** Evolution of the values of  $I_l$  and  $\gamma_l$  ( $l = 1, 2$ ) at  $s = 2000$  for RF (a) and LF (b) pulses:  $I_l$  (thick lines),  $\gamma_l$  (thin lines).

intensity form at their trailing edges. Figure 2 shows a more detailed structure of these trains at  $s = 2000$ . The durations of RF pulses 1 and 2 in Fig. 2, a are about 180 and 90 ps, respectively. The peak intensity of pulse 1 is approximately  $7 \text{ kW/cm}^2$ . The durations of LF pulses 1 and 2 in Fig. 2, b are 160 and 90 ps, respectively; the peak intensity of pulse 2 is  $17 \text{ kW/cm}^2$ . Figure 3, a shows the intensity envelopes of both pulses 1 from Figs. 2, a and 2, b, while Fig. 3, b presents the intensity envelopes of both pulses 2 from the same figures. Figure 3 demonstrates that subpulses of RF and LF fields are located in pairs in the

same space-time domain and, therefore, interact with each other.

(B) Input pulses identical in polarization direction. Let us set  $\tau_0 = 100$  and  $\gamma_{10} = 1$  in (3). In this case, the input RF and LF pulses have left circular polarization and the same duration. Figure 4 shows plots of the values of  $I_l$  and  $\gamma_l$  ( $l = 1, 2$ ) for several distances  $s$ . Dashed lines represent the values of  $I_{l0}$  ( $l = 1, 2$ ), which is the intensity of reference pulses. Figure 4 demonstrates that, as in the case of opposite polarizations of input radiation, the RF pulse is damped during propagation, while the LF pulse

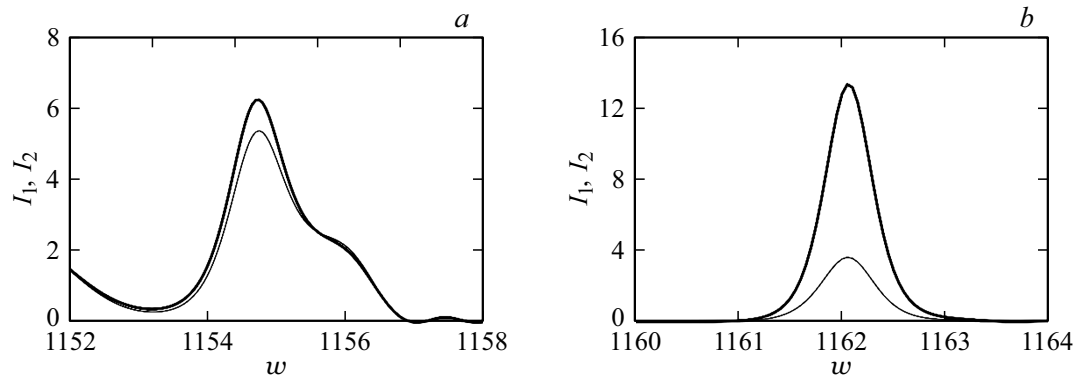


**Figure 3.** Evolution of the values of  $I_1$  (thin lines) and  $I_2$  (thick lines) for pulses 1 (a) and pulses 2 (b) at  $s = 2000$ .

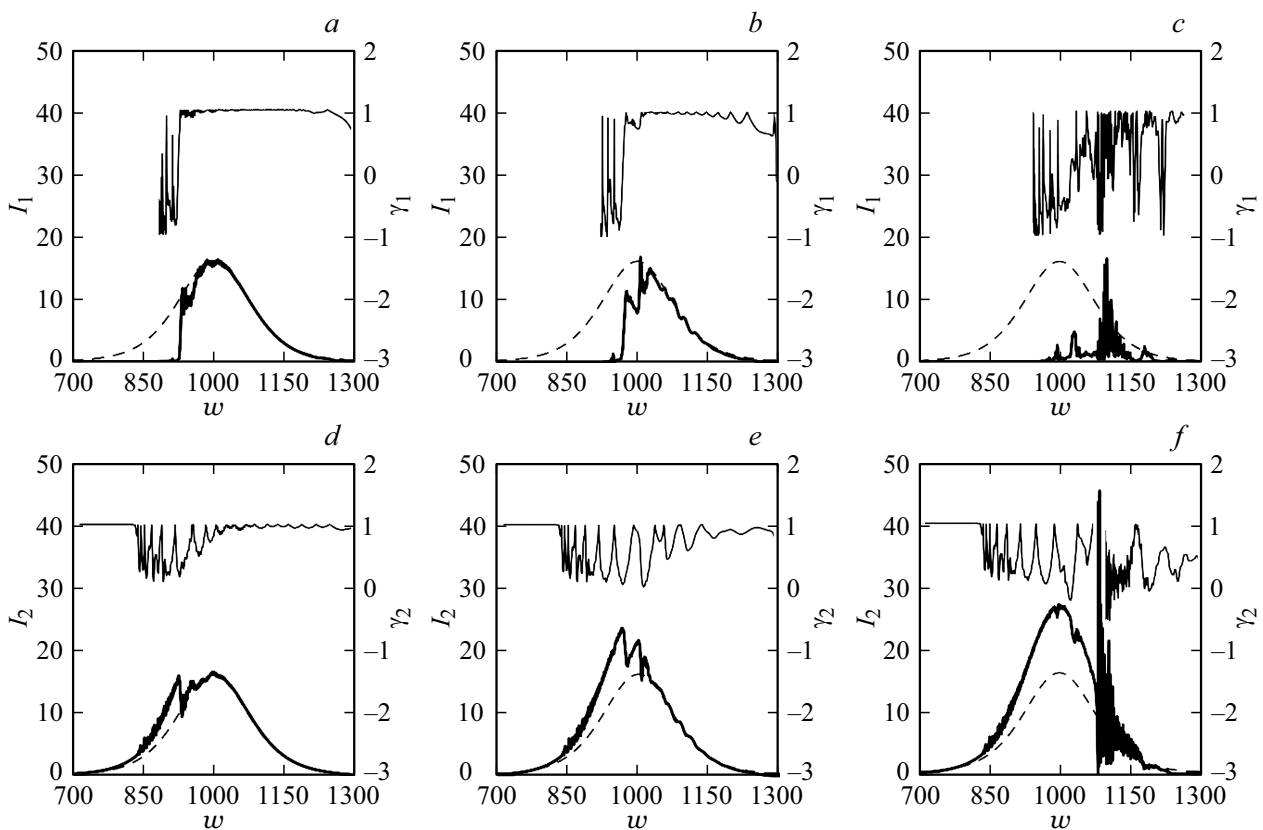


**Figure 4.** Evolution of the values of  $I_1$  (thick lines),  $\gamma_1$  (thin lines), and  $I_{10}$  (dashed lines) at  $s = 200$  (a),  $400$  (b), and  $800$  (c); evolution of the values of  $I_2$  (thick lines),  $\gamma_2$  (thin lines), and  $I_{20}$  (dashed lines) at  $s = 200$  (d),  $400$  (e), and  $800$  (f).

is amplified. However, the distance of attenuation of the RF pulse is now much shorter than in the case of input pulses with different directions of circular polarizations. Moreover, at large distances, this pulse decays into a set of subpulses (Fig. 4,c) that cannot be resolved on the scale of this figure. At large values of distance  $s$ , a train of subpulses (also unresolved) appears at the trailing edge of the LF pulse (Fig. 4,f). The peak intensity of some pulses of this train is almost three times higher than the peak intensity of the input LF pulse and reaches  $60 \text{ kW/cm}^2$ . Figure 4 indicates that, unlike the case of

identical polarization directions of the input radiations, the values of  $\gamma_l$  ( $l = 1, 2$ ) depend significantly on time. This leads to similar dependences of the PE eccentricities of both pulses.

Figure 5 shows the evolution of  $I_l$ ,  $\alpha_l$  and  $\gamma_l$  ( $l = 1, 2$ ) in the central part of the RF pulse (Fig. 5,a) and in the region of the LF pulse train (Fig. 5,b) at  $s = 800$ . According to Fig. 5,a, the RF field is a set of chaotically arranged subpulses with the average distance between their peaks being around 240 ps. The most intense subpulse has a peak value of about  $20 \text{ kW/cm}^2$  and a duration of about 60 ps.

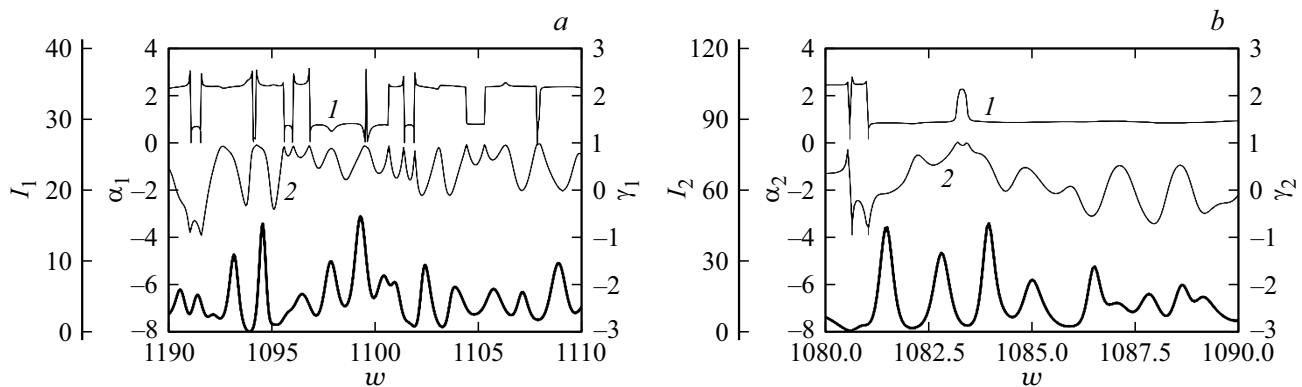


**Figure 5.** Evolution of  $I_l$ ,  $\alpha_l$  and  $\gamma_l$  ( $l = 1, 2$ ) at  $s = 800$  for RF (a) and LF (b) pulses:  $I_l$  — thick lines,  $\alpha_l$  — curves 1, and  $\gamma_l$  — curves 2.

Quantity  $\alpha_1$  (curve 1) varies in  $\pm\pi$  steps due to the limitation on the range of its values. However, there are also jump transitions with an absolute magnitude smaller than  $\pi$ . Jumps of this type occur at the moment when  $\gamma_1 = 1$ , i.e. at the moment when the PE converges to a circle. Therefore, the continuity of PE evolution is not disturbed by such jumps. The value of  $\gamma_1$  (curve 2) varies from 0 to 1 within the greater part of Fig. 5, a. This means that the polarization state of RF radiation changes from linear to circular. The duration of subpulses at the trailing edge of the LF pulse (Fig. 5, b) is approximately 100 ps, quantity  $\alpha_2$  remains constant over most of the train ( $\alpha_2 = 0.735$ ), and the value of  $\gamma_2$  varies approximately from  $-0.4$  to  $+1$ . Consequently, the principal axis of PE radiation does not change its orientation within the greater part of the train, but its shape changes from right elliptical to left circular.

The calculation showed that the propagation of pulses in the medium is accompanied by the emergence of significant PM in the areas where subpulse trains are located. The instantaneous frequency shift in these regions exceeds the half-width of the inhomogeneous broadening line of the RF transition. In other parts of pulses, the instantaneous frequency shift is insignificant and amounts to a few percent of this half-width.

### Input pulses of different duration

(A) Input pulses with opposite polarization directions. Let us set  $\tau_0 = 200$  and  $\gamma_{10} = -1$  in (3). In this case, the input RF pulse has twice the duration of the input LF pulse and the directions of circular polarizations of these pulses are opposite to each other. Figure 6 shows plots of the values of  $I_l$  and  $\gamma_l$  ( $l = 1, 2$ ) for several distances  $s$ . The plots of  $\alpha_l$  and  $\delta_{x,l}$  are not presented, since these quantities remain constant and equal to their values for the input pulses. According to Fig. 6, the same property holds for  $\gamma_l$ . This means that both radiations propagating in the medium remain circularly polarized and devoid of PM, just as in the case of equal in duration input pulses with opposite circular polarizations (Fig. 1). According to Fig. 6, the

envelopes of pulse intensities deform significantly during propagation. A comparison of Fig. 6 and Fig. 1 shows that the subpulse trains appearing at the trailing edges of RF pulses at a large distance ( $s = 2000$ ) are much more intense in the case of different input pulse durations than in the case of their identical duration. At  $1500 < s < 2000$ , the smooth maximum of the RF pulse envelope located before the subpulse train (Fig. 6, c) propagates at a velocity about 35 times lower than  $c$ .

(B) Input pulses identical in polarization direction. Let us set  $\tau_0 = 200$  and  $\gamma_{10} = 1$  in (3). This corresponds to the case where the input RF pulse has twice the duration of the input LF pulse and the circular polarization directions of these pulses are the same. Figure 7 shows plots of the values of  $I_l$  and  $\gamma_l$  ( $l = 1, 2$ ) for several distances  $s$ . Note that, as in all previous cases, the shape of curves  $I_1$  is subject to considerable distortion. Already at a distance of  $s = 1500$ , the RF pulse decays into trains of subpulses, transferring almost all of its energy to the LF field pulse. A train of intense subpulses (similar to the trains discussed in the above paragraphs) is formed at the trailing edge of the RF field pulse. Quantities  $\alpha_l$  and  $\gamma_l$  ( $l = 1, 2$ ) vary significantly. The calculation shows that similar changes are characteristic of the values of  $\alpha_l$  and  $\delta_{x,l}$  ( $l = 1, 2$ ). Consequently, the shape and orientation of the PE of both radiations change at each point of the resonant medium.

### Energy characteristics of pulses in the medium

We define the value of  $Tr(s)$  as  $Tr(s) = W(s)/W(0)$ , where  $W(s)$  is the amount of energy carried by the pulse through a unit area of the cross section located at distance  $s$  from the input surface within the time of pulse propagation through that section. Quantity  $Tr(s)$  indicates the relative change in input pulse energy over distance  $s$  from the input surface. Figure 8 shows plots of this quantity for the cases of identical (Fig. 8, a) and different (Fig. 8, b) input pulse durations at opposite (thick lines) and identical (thin lines) directions of circular polarizations of input radiations. According to Fig. 8, when pulses propagate

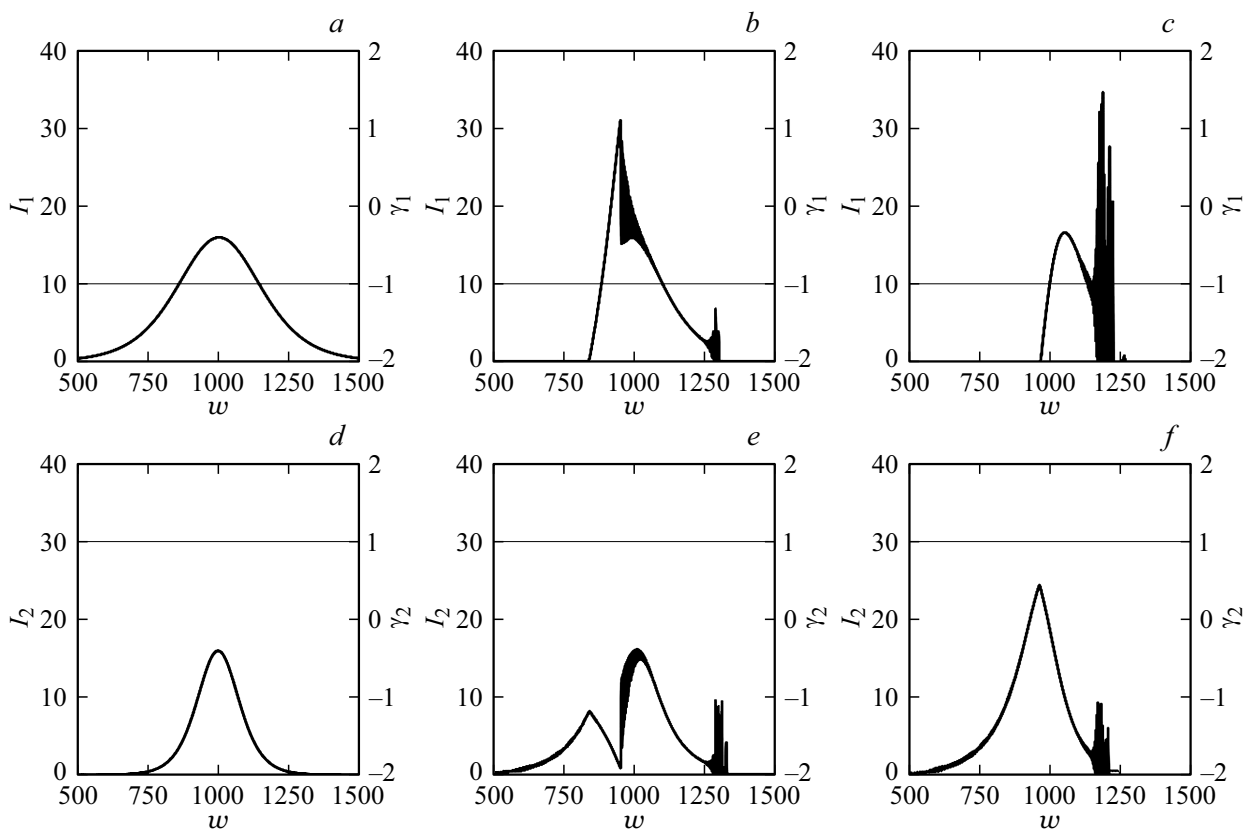


**Figure 6.** Evolution of the values of  $I_1$  (thick lines) and  $\gamma_1$  (thin lines) at  $s = 0$  (a), 500 (b), and 2000 (c); evolution of  $I_2$  (thick lines) and  $\gamma_2$  (thin lines) at  $s = 0$  (d), 500 (e), and 2000 (f).

in the medium, the RF pulse energy is pumped into a pulse of LF radiation. A comparison of the thick and thin curves in Figs. 8, *a* and *b* shows that this process is slower in the case of opposite directions of circular polarizations of the input pulses than when their circular polarizations are the same. Therefore, in the first case, the RF pulse penetrates into the medium to a greater distance than in the second case. At sufficiently large distances, the RF pulse vanishes, and the LF pulse propagates without energy change. The calculation shows that about 20 and 25% of the total energy of radiation is lost in the medium in the case of equal and different durations of input pulses, respectively. The mentioned energy losses are related to relaxation decay of the upper levels of the considered  $\Lambda$  scheme.

The physical reason for the situation described above is as follows. According to the rules of selection by quantum number  $M$ , quantum transitions between states  ${}^3P_0$  ( $M = 0$ ),  ${}^3P_1^0$  ( $M = 1$ ), and  ${}^3P_2$  ( $M = 2$ ) of the lower, upper, and middle energy levels are involved in interaction with the field in the case of opposite circular polarizations of input pulses. For the same circular polarization directions of the input pulses, these states are  ${}^3P_0$  ( $M = 0$ ),  ${}^3P_1^0$  ( $M = -1$ ), and  ${}^3P_2$  ( $M = 0$ ), respectively. In both cases, the magnitudes of dipole moments of transitions between the states of the lower and upper energy levels are equal. However, in the first case, the squared modulus of the

dipole moment of the transition between the states of the middle and upper levels is five times greater than in the second case [35]. According to the EIT [4–6] theory, the depth of RF pulse penetration into the medium increases in proportion to the square of the dipole moment of the transition between excited states of the  $\Lambda$  scheme. Therefore, in the case of opposite circular polarizations of input pulses, the RF pulse penetrates deeper than in the case of identical polarization directions of these pulses. Note that the theory of ideal EIT relies on the assumption of counterintuitive [4] excitation of quantum transitions that is realized in the case when the input LF pulse arrives to an input surface of the medium before the RF pulse. In the situation we are considering, this condition is obviously not fulfilled, and EIT proceeds in conditions that are not ideal for this phenomenon.

## Conclusion

The calculation results show that the evolution of co-propagating resonant pulses with different frequencies essentially depends on their polarizations on entrance to the medium. Even in the case of comparable intensities and durations of input radiations, a significant EIT effect associated with the creation of coherence at the transition between the upper energy levels of the  $\Lambda$  scheme is

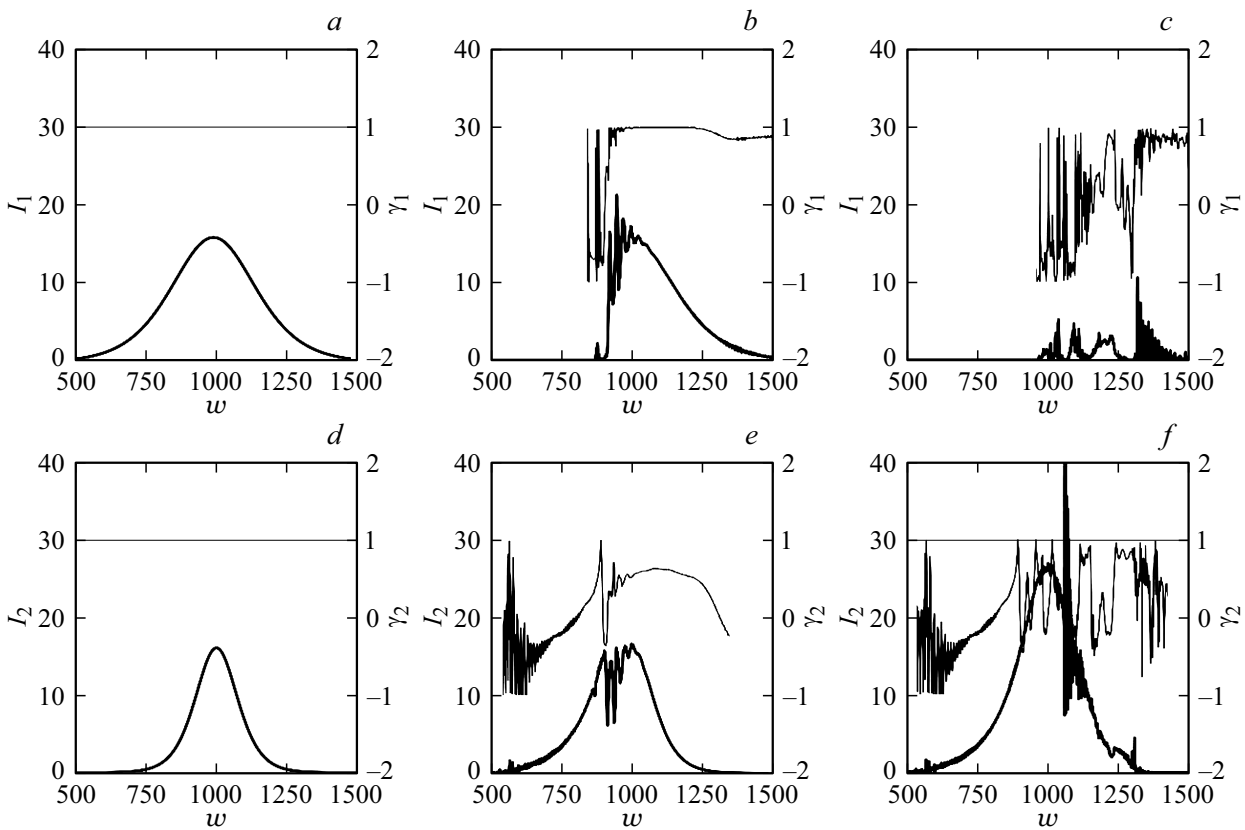


**Figure 7.** Evolution of  $I_1$  (thick lines) and  $\gamma_1$  (thin lines) at  $s = 0$  (a), 500 (b), and 1500 (c); evolution of  $I_2$  (thick lines) and  $\gamma_2$  (thin lines) at  $s = 0$  (d), 500 (e), and 1500 (f).

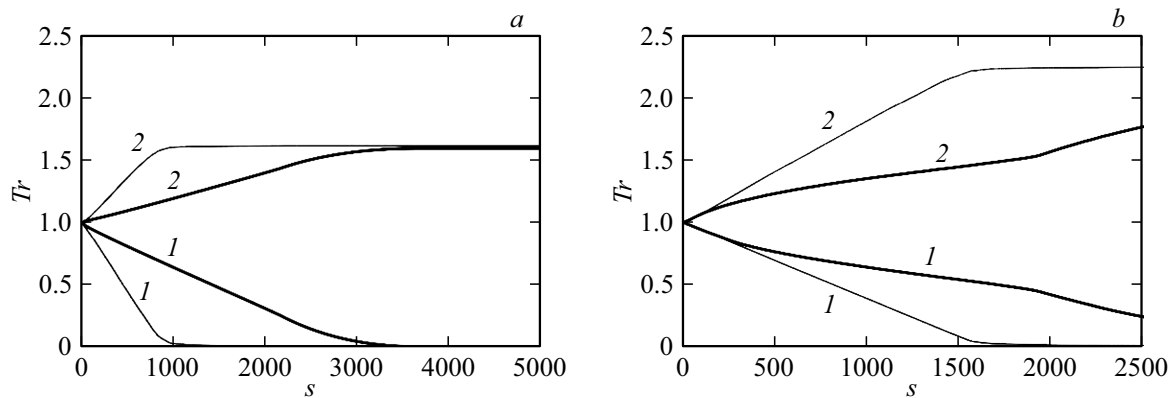


**Figure 8.** The dependence of  $Tr$  on  $s$  in the case of equal (a) and different (b) input pulse durations at different (thick lines) and identical (thin lines) directions of their circular polarizations; curves 1 — RF radiation, curves 2 — LF radiation.

manifested in this context. In the case of opposite circular polarizations of input pulses, the influence of coherence on the pulse propagation process is greater than in the case of identical directions of these polarizations. Therefore, in the first case, the pulses propagate in the medium for longer distances and experience smaller deformations than when their circular polarizations have the same direction. In addition, in the first case, the polarization characteristics of radiations remain unchanged in the medium; in the second case, these characteristics

change significantly. However, in all situations, trains of short bell-shaped subpulses form at the trailing edges of pulses. This is explained by the non-stationarity of the process of interaction of radiation with the medium. Note that subpulse trains also emerge when the input RF pulse is much shorter than the input LF pulse [32]. However, the intensity of subpulses under these conditions is much smaller than that of trains in the calculations presented above.

## Conflict of interest

The authors declare that they have no conflict of interest.

## References

- [1] W. Demtröder. *Laser Spectroscopy* (Springer, 2008).
- [2] B.D. Agap'ev, M.B. Gornyi, B.G. Matisov, Yu.V. Rozhdestvenskii. *Phys.-Usp.*, **36** (9), 763 (1993).
- [3] E. Arimondo. *Progress in Optics*, **35**, 257 (1996).
- [4] S.E. Harris. *Phys. Today*, **50** (6), 36 (1997).
- [5] M.D. Lukin. *Rev. Mod. Phys.*, **75** (2), 457 (2003).
- [6] M. Fleischhauer, A. Imamoglu, J.P. Marangos. *Rev. Mod. Phys.*, **77** (2), 633 (2005).
- [7] L.-M. Duan, M.D. Lukin, J.I. Cirac, P. Zoller. *Nature (London)*, **414**, 413 (2001).
- [8] A. Sinatra. *Phys. Rev. Lett.*, **97** (25), 253601 (2006).
- [9] M. Martinelli, P. Valente, H. Failache, D. Felinto, L.S. Cruz, P. Nussenzeig, A. Lezama. *Phys. Rev. A*, **69** (4), 043809 (2004).
- [10] A. Godone, S. Micallizio, F. Levi. *Phys. Rev. A*, **66** (6), 063807 (2002).
- [11] M.D. Lukin, A. Imamoglu. *Nature (London)*, **413**, 273 (2001).
- [12] O. Kocharovskaya, P. Mandel. *Phys. Rev. A*, **42** (1), 523 (1990).
- [13] H.H. Jen, Daw-Wei Wang. *Phys. Rev. A*, **87** (6), 061802(R) (2013).
- [14] C. Basler, J. Grzesiak, H. Helm. *Phys. Rev. A*, **92** (1), 013809 (2015).
- [15] Ronggang Liu, Tong Liu, Yingying Wang, Yujie Li, Bingzheng Gai. *Phys. Rev. A*, **96** (5), 053823 (2017).
- [16] Fam Le Kien, A. Rauschenbeutel. *Phys. Rev. A*, **91** (5), 053847 (2015).
- [17] Hai-Hua Wang, Jing Wang, Zhi-Hui Kang, Lei Wang, Jin-Yue Gao, Yi Chen, Xiao-Jun Zhang. *Phys. Rev. A*, **100** (2), 013822 (2019).
- [18] M.J. Konopniki, J.H. Eberly. *Phys. Rev. A*, **24** (5), 2567 (1981).
- [19] A. Rahman, J.H. Eberly. *Phys. Rev. A*, **58** (2), R.805 (1998).
- [20] R. Grobe, J.H. Eberly. *Laser Phys.*, **29** (3), 542 (1995).
- [21] S.E. Harris. *Phys. Rev. Lett.*, **70** (5), 552 (1993).
- [22] A.M. Basharov, A.I. Maimistov. *J. Exp. Theor. Phys.*, **67** (12), 2426 (1988).
- [23] A.M. Basharov. *Izv. Ross. Akad. Nauk, Ser. Fiz.*, **66** (3) 357 (2002) (in Russian).
- [24] R. Grobe, F.T. Hioe, J.H. Eberly. *Phys. Rev. Lett.*, **73** (24), 3183 (1994).
- [25] S. Wielandy, A.L. Gaeta. *Phys. Rev. Lett.*, **81** (16), 3359 (1998).
- [26] Bo Wang, Shujing Li, Jie Ma, Hai Wang, K.C. Peng, Min Xiao. *Phys. Rev. A*, **73** (5), 051801(R) (2006).
- [27] Z. Kis, G. Demeter, J.J. Janszky. *Opt. Soc. Am. B*, **30** (4), 829 (2013).
- [28] O.M. Parshkov. *Quantum Electron.*, **48** (11), 1027 (2018).
- [29] V.G. Arkhipkin, I.V. Timofeev. *Phys. Rev. A*, **64** (5), 053811 (2001).
- [30] A. Kasapi, Maneesh Jain, G.Y. Yin, S.E. Harris. *Phys. Rev. Lett.*, **74** (13), 2447 (1995).
- [31] Maneesh Jain, A. Kasapi, G.Y. Yin, S.E. Harris. *Phys. Rev. Lett.*, **75** (4), 4385 (1995).
- [32] O.M. Parshkov. *Kvantovaya Elektron.*, **52** (8), 720 (2022) (in Russian).
- [33] S.E. Harris, Zhen-Fei Luo. *Phys. Rev. A*, **52** (2), R928 (1995).
- [34] Yong-ging Li, Min Xiao. *Phys. Rev. A*, **51** (6), 4959 (1995).
- [35] R.L. de Zafra, A. Marshall. *Phys. Rev.*, **170** (1), 28 (1968).
- [36] *Fizicheskiye velichiny. Spravochnik*, Ed. by I.S. Grigor'ev, E.Z. Meilikhov (Energoatomizdat, M., 1991) (in Russian).

Translated by D.Safin